

# Identification of Single-Atom Active Sites in CO Oxidation Over Oxide-Supported Au Catalysts

Christian Schilling<sup>1†</sup>, Marc Ziemba<sup>1†</sup>, Christian Hess<sup>1\*</sup>, M. Verónica Ganduglia-Pirovano<sup>2\*</sup>

<sup>1</sup>Eduard-Zintl-Institut für Anorganische und Physikalische Chemie, Technische Universität  
Darmstadt, Alarich-Weiss-Str. 8, 64287 Darmstadt, Germany

<sup>2</sup>Instituto de Catálisis y Petroleoquímica–Consejo Superior de Investigaciones Científicas,  
Marie Curie 2, 28049 Madrid, Spain

<sup>†</sup>Both authors contributed equally

## Keywords

Single site catalysis, gold, CO oxidation, *operando* infrared spectroscopy, density functional  
theory

## **Abstract**

Here we present a combined *operando* infrared spectroscopic and theoretical analysis of ceria-supported gold catalysts during room temperature CO oxidation that identifies an active site for the reaction as a single gold site on the ceria support forming an  $O_{\text{lattice}}\text{-Au}^+\text{-CO}$  species. As monitored by *operando* infrared spectroscopy, the isolated  $\text{Au}^+$  gold site is either present as a result of the catalyst synthesis or formed under reaction conditions after CO adsorption at the perimeter of the Au–ceria interface. Our results provide new insights into the chemical nature of the active gold site and the reaction mechanism by detecting the formation of active and inhibiting species simultaneously.

## 1. Introduction

Strongly interacting gold with an oxide support has aroused a great deal of attention as a catalyst since its discovery,<sup>1,2</sup> owing to its high reactivity for a number of important reactions,<sup>3</sup> such as CO oxidation,<sup>4</sup> water–gas shift,<sup>5</sup> acetylene hydrochlorination,<sup>6</sup> and preferential oxidation of CO.<sup>7</sup> The use of reducible oxides, such as ceria (CeO<sub>2</sub>), as a support for Au catalysts, has been found to lead to highly active catalytic systems for numerous reactions, e.g., CO oxidation<sup>4</sup> and water–gas shift<sup>5</sup>. However, despite extensive research on ceria-supported gold catalysts (Au/CeO<sub>2</sub>) in the past,<sup>8-15</sup> even for a seemingly simple reaction such as CO oxidation, the nature of the active catalytic site as well as other important details of the reaction mechanism, such as the role of water/hydroxide, are still under debate.<sup>16-24</sup>

Previous work on CO oxidation over ceria-supported Au nanoparticles has shown that the Au–oxide interfacial perimeter plays a major role<sup>25</sup> and that the oxygen activation proceeds at the ceria support<sup>12</sup> via peroxide formation at ceria defect sites<sup>13-15</sup>. On the other hand, there is controversy in the literature regarding whether the active gold sites are gold clusters or interfacial gold atoms, or isolated cationic gold ions, or a mixture of different sites.<sup>16</sup> More recently, based on *in situ* X-ray absorption fine structure analysis, the metallic gold component in the ceria-supported Au clusters has been proposed to play a crucial role in the catalysis,<sup>18</sup> in contrast to recent theoretical work reporting the formation of cationic gold ions<sup>17</sup> or dimeric gold species<sup>26</sup> as catalytically active sites, however, without providing experimental evidence for the existence of such species in either report. Previous calculations on Au<sub>1</sub><sup>27</sup>, Au<sub>3</sub><sup>28</sup>, Au<sub>13</sub><sup>29</sup>, and Au<sub>20</sub><sup>25</sup> have predicted that oxidized gold species – in direct contact with the ceria support – are the preferred sites for CO adsorption. CO bound to oxidized gold species has also been reported for other oxides such as ZnO and TiO<sub>2</sub>.<sup>30,31</sup> Not long ago, the structural changes of Au(111) and Au ceria-supported small (~2 nm) gold clusters have been demonstrated by employing *in situ* STM<sup>32</sup> and environmental transmission electron microscopy<sup>33</sup> in the presence of CO at reduced pressures (~10<sup>-4</sup> mbar).

In this contribution, we report on the identification and characterization of an active site in ceria-supported gold catalysts in CO oxidation. We show that infrared spectroscopy enables the monitoring of the active sites and inhibiting species as well as their formation behavior. Assignment of vibrational frequencies based on DFT calculations allows detailed insight into the active site of supported gold catalysts. In particular, our results provide clear evidence that isolated cationic  $\text{Au}^+$  in close interaction with the support are creating active  $\text{O}_{\text{lattice}}-\text{Au}^+-\text{CO}$  species during CO oxidation over ceria supported gold catalysts.

## 2. Methods

**Catalyst preparation.** Ceria nanoparticles were prepared by decomposition of  $\text{Ce}(\text{NO}_3)_3 \cdot 6 \text{H}_2\text{O}$  (99.5 %, Alfa Aesar) at  $600^\circ\text{C}$  for two periods of 12 h and were thoroughly characterized as described elsewhere.<sup>15,34</sup> Please note that the ceria nanoparticles possess a termination in the (111) direction as well as stepped sites, as is evident from transmission electron microscopy data and *in situ* Raman spectra. Therefore, the experimental results are directly comparable to the DFT calculations employing (111)-oriented ceria slabs. Au/CeO<sub>2</sub> samples with 0.5 wt% Au loading were synthesized via deposition precipitation from  $\text{HAuCl}_4 \cdot 3 \text{H}_2\text{O}$  (> 99.99 %, Sigma Aldrich). An *ex situ* characterization of the gold content and the oxidation state has already been carried out in earlier work by XP spectroscopy and is described there in more detail.<sup>15,34</sup> TEM studies have revealed the presence of a small number of larger gold particles (~10 nm).<sup>15</sup> However, as discussed previously, the catalytic activity of the Au/ceria catalyst is attributed to highly dispersed gold rather than the particles we observe in TEM.<sup>15</sup>

**Operando IR spectroscopy.** We used diffuse reflectance infrared Fourier transform spectroscopy (DRIFTS) in a Vertex 70 (Bruker) to examine a 0.5 wt% Au/CeO<sub>2</sub> catalyst exposed to reaction conditions. Gas phase infrared analysis was employed to quantitatively

monitor the conversion over the catalyst and can be directly correlated with the spectroscopic information gained from infrared spectroscopy at the catalyst (*operando* approach). For further details, refer to the Supporting Information and reference 42.

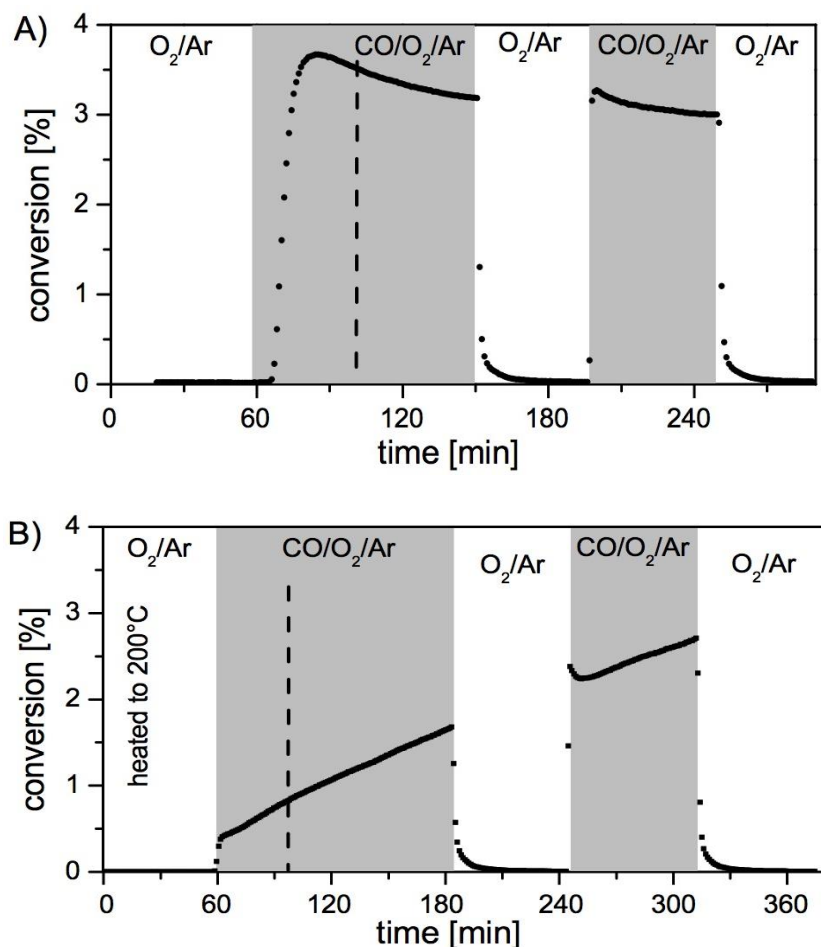
**Density functional theory (DFT).** Density functional theory calculations were performed employing the VASP package (version 5.3.5 <https://www.vasp.at>) with the PBE functional adding an effective onsite Coulomb interaction parameter  $U_{\text{eff}} = 4.5$  eV for the Ce 4*f* states (PBE+U/4.5 eV) and a hybrid DFT functional (HSE06). Vibrational analyses were performed by calculating the Hessian either analytically or with a finite differences approach. For further details, refer to the Supporting Information and reference 35.

### 3. Results and Discussion

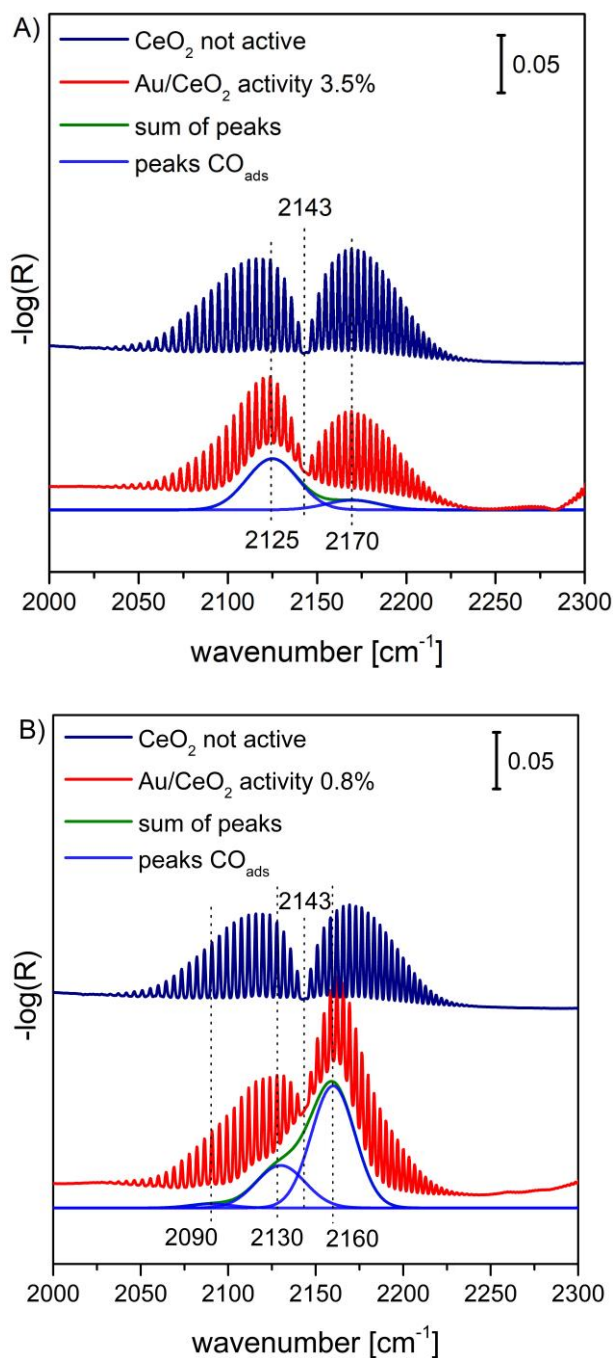
**Catalytic activity.** The Au/CeO<sub>2</sub> catalyst contains a gold loading of 0.5 wt% prepared by deposition precipitation onto polycrystalline CeO<sub>2</sub> exhibiting a (111) termination (see Supporting Information for details of the synthesis and characterization). Figure 1 depicts the temporal evolution of the conversion over the 0.5 wt% Au/CeO<sub>2</sub> catalyst during CO oxidation at 21°C for two different catalyst pretreatments (A and B in Figure 1A and 1B, respectively) prior to exposure to reaction conditions. Pretreatment A consists of equilibration in 25% O<sub>2</sub>/Ar flow for 1 h, whereas pretreatment B involves an outgassing step at 200°C (25% O<sub>2</sub>/Ar flow, 1 h), leading to the removal of adsorbed water. After equilibration, the as-prepared catalyst starts to show activity after 5 min in reaction conditions, reaching maximum conversion after 20 min, and then slowly declines to the steady-state conversion (~3%). In contrast, after outgassing at 200°C, the catalyst activates only slowly (2 h) without reaching steady-state conversion. This activation process continues after a regeneration phase in 25% O<sub>2</sub>/Ar for 1 h (Figure 1). The steady-state conversion of ~3% after equilibration is not reached even after

exposure to reaction conditions for 3 h. Such a prolonged activation period has been observed previously for room temperature CO oxidation in dry reaction gas streams and has been assigned to the positive influence of water on the activation behavior of Au/CeO<sub>2</sub> catalysts.<sup>36</sup>

**Catalyst behavior under reaction conditions.** To explore the behavior of the catalyst under reaction conditions, we performed *operando* infrared spectroscopy during the course of the reactivity experiment in Figure 1 by recording spectra every minute. Exemplary *operando* infrared spectra during reaction (dashed lines in Figure 1) are depicted in Figure 2 (red spectra) showing an excerpt of the CO stretching mode region. The rotational–vibrational fine structure of CO can be resolved in the infrared spectra (1 cm<sup>-1</sup> resolution), and thus gas-phase CO molecules, possessing a rotational–vibrational fine structure, are distinguished from vibrations of adsorbed CO, which do not possess a fine structure. On the bare ceria support (blue spectra) no adsorbed CO species are observed under reaction conditions, which were detected in the region 2154–2177 cm<sup>-1</sup> in prior CO adsorption experiments by stabilization at lower temperatures and reduced pressures.<sup>37-40</sup> After subtraction of the gas-phase spectrum from the spectrum of the Au/CeO<sub>2</sub> catalyst, the residual signal can be de-convoluted into three distinct spectral regions at i) 2125–2130 cm<sup>-1</sup> (present for all active samples), ii) 2160–2170 cm<sup>-1</sup> (present for all samples, but with a very different intensity), and at iii) 2090 cm<sup>-1</sup> (low intensity, only present for the outgassed sample).



**Figure 1:** Conversion (CO oxidation) over a 0.5 wt% Au/CeO<sub>2</sub> catalyst during two exposures to reaction conditions (2% CO, 10% O<sub>2</sub>, Ar) at 21°C after **A)** 25% O<sub>2</sub>/Ar flow for 1 h and **B)** 25% O<sub>2</sub>/Ar flow at 200°C for 1 h. The dashed line indicates the time of the infrared spectroscopy measurement during reaction depicted in Figures 2 and 4 as well as in Figures S1 and S2.



**Figure 2:** CO stretch frequency region of the *operando* infrared spectra under reaction conditions (red) after **A)** equilibration in 25% O<sub>2</sub>/Ar flow and **B)** outgassing in 25% O<sub>2</sub>/Ar at 200°C for 1 h. Subtraction of the infrared spectrum of gas-phase CO over a bare CeO<sub>2</sub> sample (no adsorbed CO, dark blue) yields the residual spectrum (green), which can be deconvoluted into three components at 2160–2170 cm<sup>-1</sup>, 2125–2130 cm<sup>-1</sup>, and 2090 cm<sup>-1</sup>.



**Identification of active sites.** For a detailed assignment of the experimentally observed CO stretch frequencies, the CO chemisorption and vibrational properties on model Au-CeO<sub>2</sub> catalysts consisting of single Au<sub>1</sub> and Au<sub>4</sub> gold clusters adsorbed on CeO<sub>2</sub>(111) surface were calculated employing DFT (Figure 3) with either PBE+U/4.5 eV or hybrid HSE06 exchange-correlation functionals. The PBE+U/4.5 eV functional revealed comparable results independently of whether van der Waals (vdW) contributions were considered, and thus vdW contributions were not included in combination with HSE06 (see Supporting Information). All computational frameworks predict that the most stable Au<sub>1</sub> site is an O–O bridge (Au@O–O bridge), in which the Au 6s electron is transferred to the ceria support (Au<sup>+</sup>), accompanied by the formation of a Ce<sup>3+</sup> ion in a next nearest neighbor (NNN) cationic position to the Au atom (Figure 3D), in agreement with previous results.<sup>41-45,27,28</sup>

With respect to ceria-supported Au<sub>4</sub> clusters, a pyramidal-shaped cluster has been predicted to be the most stable configuration for adsorption on either the stoichiometric CeO<sub>2</sub>(111)<sup>28,46</sup> or the reduced CeO<sub>2-x</sub>(111) surfaces<sup>47</sup>. In the case of the CeO<sub>2</sub>(111) surface, two Ce<sup>3+</sup> ions – resulting from the Au-ceria interaction – are located in nearest neighbor (NN) cationic positions to the Au<sub>4</sub> cluster (Figure 3M); hence, we have adopted such a Ce<sup>3+</sup> configuration for the Au<sub>4</sub>/CeO<sub>2</sub>(111)<sup>48,28</sup> system with a pyramidal-shaped Au<sub>4</sub> cluster in which the bottom three Au atoms – in direct contact with the ceria support – are charged positively (Au<sup>+0.67</sup>), whereas the gold atom at the top is practically not charged (Au<sup>0</sup>), see Table S3.<sup>28</sup> Thus, there is a rapid weakening of the Au-ceria interactions as clusters become three-dimensional, in line with previous findings for other metals such as Ni.<sup>48,49</sup> In this context, other Au<sub>4</sub>/CeO<sub>2</sub>(111) structures were also considered in which, for example, there are two Ce<sup>3+</sup> ions in next-nearest cationic positions (NNN) to the Au<sub>4</sub> cluster; however, all of these structures were found to be higher in energy and were not considered further.

For Au<sub>1</sub>/CeO<sub>2</sub>(111), upon CO adsorption on the gold atom, the formation of O<sub>lattice</sub>–Au<sup>+</sup>–CO species is observed (Table 1 and Table S3), regardless of the starting structure, the

charge state of gold, or the employed computational framework (see Supporting Information). The CO molecule is adsorbed on top of the Au<sup>+</sup> ion at O–O bridge sites in an almost upright position forming a linear O<sub>lattice</sub>–Au<sup>+</sup>–CO species (only slightly tilted for the Ce<sup>3+</sup> localization in a NN position), with an adsorption energy of  $E_{\text{ads,CO}} = -2.43$  and  $-2.30$  eV (HSE06) for the Au@O–O bridge structure with the Ce<sup>3+</sup> in NNN and NN positions, respectively (Figures 3I and 3J, and Table S3).

For CO adsorption on the Au<sub>4</sub>/CeO<sub>2</sub>(111) cluster, three different adsorption sites are possible:

(i) On top of the gold atom at the apex of the pyramid (Au<sub>top</sub>) with an adsorption energy of  $E_{\text{ads,CO}} = -0.77$  eV (HSE06) and a linear upright adsorption geometry (Table 1 and Figure 3N).

(ii) On the gold atom in the base that has two Ce<sup>3+</sup> in NN positions (Au<sub>bottom,1</sub>) with an adsorption energy of  $E_{\text{ads,CO}} = -1.26$  eV (HSE06). Interestingly, the Au<sub>bottom,1</sub> atom, onto which CO is adsorbed, is abstracted from the Au<sub>4</sub> cluster, forming a *pseudo single Au site*, i.e., an O<sub>lattice</sub>–Au<sup>+</sup>–CO species slightly separated from the remaining Au<sub>3</sub> particle, that stays perpendicular to the surface (Table 1 and Figure 3O). The gold atom abstracted from the Au<sub>4</sub> cluster to form a O<sub>lattice</sub>–Au<sup>+</sup>–CO species (Figure 3I) has practically the same positive charge than *true* isolated species (Table S3). The abstraction of Au atoms from ceria-supported Au clusters upon CO adsorption at the Au–ceria interface has previously been reported.<sup>17,28</sup>

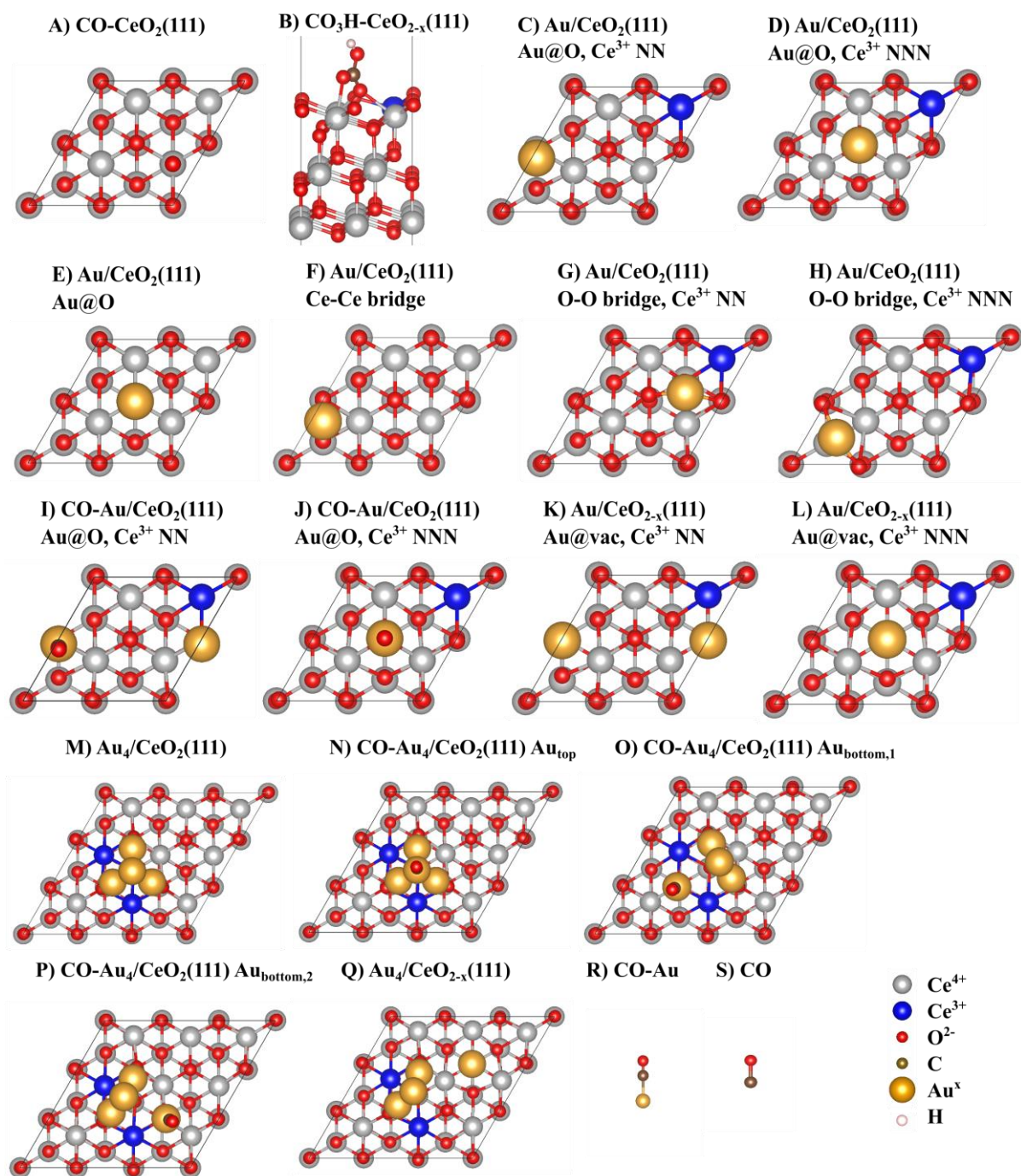
(iii) On one of the gold atoms located between nearest neighboring Ce<sup>3+</sup> and Ce<sup>4+</sup> cations (Au<sub>bottom,2</sub>) with an adsorption energy of  $E_{\text{ads,CO}} = -1.29$  eV (HSE06). Au<sub>bottom,2</sub> sites are also abstracted from the cluster upon CO adsorption (Table 1 and Figure 3P) and *pseudo single Au sites* are formed (Table S3). The corresponding  $E_{\text{ads,CO}}$  values calculated with the PBE functional for the three distinct sites in the Au<sub>4</sub> cluster (Table S1) compare well with those in the literature for either a Au<sub>4</sub><sup>28</sup>, a Au<sub>13</sub><sup>29</sup> (the Au–CO species is not abstracted from the gold particle) or a Au<sub>20</sub><sup>17</sup> cluster supported on the CeO<sub>2</sub>(111) surface.

In addition, the adsorption of CO on the clean CeO<sub>2</sub>(111) surface was also modeled (Figure 3A): CO adsorbs linearly on the clean CeO<sub>2</sub>(111) surface on top of a Ce<sup>4+</sup> ion with an adsorption energy of  $E_{\text{ads,CO}} = -0.15$  eV (HSE06), in agreement with previous studies.<sup>39,40</sup>

For a thorough analysis of the calculated C–O stretch vibrational frequency of CO adsorbed on the Au/CeO<sub>2</sub> model systems, the stretch frequency of the isolated CO molecule ( $\tilde{\nu}_{\text{CO,gas}}$ ) has also been calculated in order to determine the corresponding CO frequency shifts ( $\Delta\tilde{\nu}_{\text{CO,gas}}$ ) upon adsorption (Table 1 and Supporting Information); the calculated gas-phase CO stretch frequency is 2236 cm<sup>-1</sup> (HSE06) and the experimentally determined value is 2143 cm<sup>-1</sup> (Figure 2). Hence, the stretch frequency of CO adsorbed on the CeO<sub>2</sub>(111) surface (2251 cm<sup>-1</sup>, HSE06) corresponds to a blueshift of  $\Delta\tilde{\nu}_{\text{CO,gas}} = +15$  cm<sup>-1</sup> with respect to isolated gas-phase CO. This value is in good agreement with the corresponding shift ( $\Delta\tilde{\nu}_{\text{CO,gas}} = +17 - +27$  cm<sup>-1</sup>) of the experimental band observed at 2160–2170 cm<sup>-1</sup> (Figure 2) and thus this band is attributed to CO adsorbed on the ceria support [CO/CeO<sub>2</sub>(111)], in agreement with previous experimental results.<sup>37-40</sup> In Table 1 the structures are sorted with respect to the value of the calculated CO stretch frequency, starting with the highest frequency value that was obtained for the CO/CeO<sub>2</sub>(111) system. All structures in which CO is adsorbed on gold exhibit a redshifted frequency with respect to the frequency of gas-phase CO ( $\Delta\tilde{\nu}_{\text{CO,gas}} < 0$ ). For the Au<sub>1</sub>/CeO<sub>2</sub>(111) structure, which has an isolated Au<sub>1</sub> atom adsorbed on the CeO<sub>2</sub>(111) surface [CO-Au<sub>1</sub>/CeO<sub>2</sub>(111)], stretch frequencies of 2219 cm<sup>-1</sup> and 2217 cm<sup>-1</sup> (HSE06) are predicted for the structures with Ce<sup>3+</sup> in NN and NNN sites to Au, respectively. These values correspond to a redshift of  $\Delta\tilde{\nu}_{\text{CO,gas}} = -17$  cm<sup>-1</sup> and  $-19$  cm<sup>-1</sup>, respectively.

As mentioned above, upon CO adsorption onto either the Au<sub>bottom,1</sub> (two NN Ce<sup>3+</sup>) or Au<sub>bottom,2</sub> (one NN Ce<sup>3+</sup>) atoms at the base of the pyramidal Au<sub>4</sub> nanoparticle, pseudo-single O<sub>lattice</sub>–Au<sup>+</sup>–CO species are formed. The corresponding calculated CO stretch frequencies are 2215 cm<sup>-1</sup> and 2214 cm<sup>-1</sup> (HSE06) for the Au<sub>bottom,1</sub> and Au<sub>bottom,2</sub> sites, respectively, which are

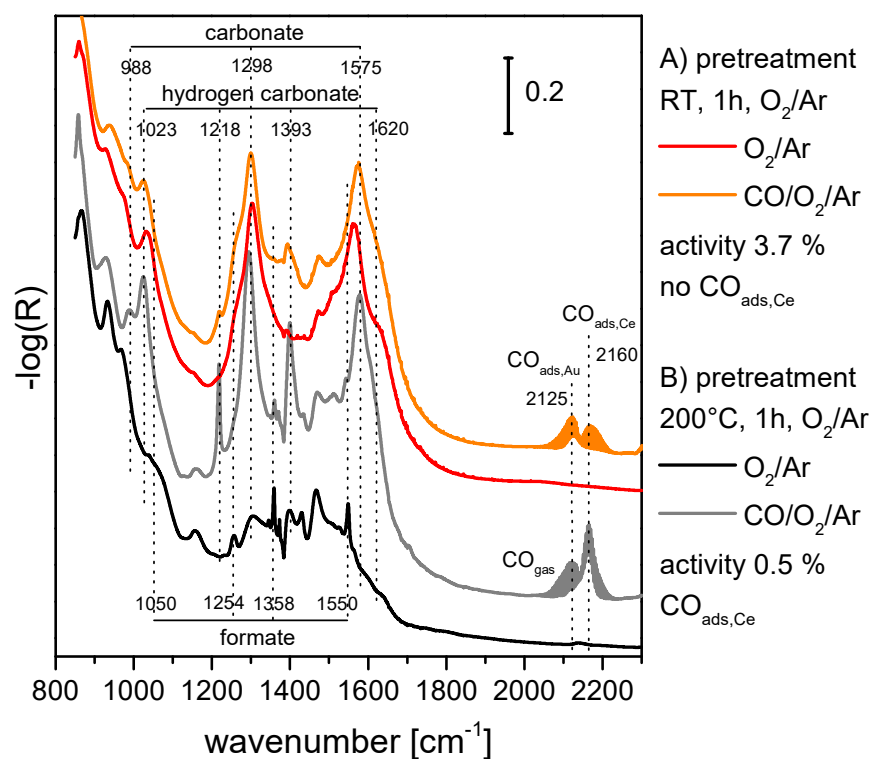
slightly redshifted ( $2\text{--}5\text{ cm}^{-1}$ ) compared to that of a (true) isolated Au site [CO-Au<sub>1</sub>/CeO<sub>2</sub>(111)]. In contrast, adsorption on top of the Au atom at the apex of the Au<sub>4</sub> cluster (Au<sub>top</sub>) revealed a stretch frequency of  $2199\text{ cm}^{-1}$  (HSE06), i.e.,  $\Delta\tilde{\nu}_{\text{CO,gas}} = -37\text{ cm}^{-1}$ . Summarizing, based on the DFT calculations, the observed CO stretch frequency at  $2125\text{--}2130\text{ cm}^{-1}$  (Figure 2) is attributed to CO adsorbed onto gold species in direct contact with the CeO<sub>2</sub> support, i.e., a O<sub>lattice</sub>-Au<sup>+</sup>-CO species. Note that, based on <sup>13</sup>CO experiments, the presence of a Ce<sup>3+</sup> related electronic transition can be ruled out (see Supporting Information, Figure S1).<sup>50</sup> The CO-related feature at  $2160\text{--}2170\text{ cm}^{-1}$  is attributed to CO adsorbed on the ceria support, and that at  $2090\text{ cm}^{-1}$  to CO adsorbed on-top of a gold atom of 3D Au clusters which are not in direct contact with the support.



**Figure 3:** Structural model of A) CO adsorbed to CeO<sub>2</sub>(111), B) adsorbed hydrogen carbonate on CeO<sub>2-x</sub>(111) with Ce<sup>3+</sup> in NNN position, Au adsorbed on-top of O (Au<sup>+</sup>@O) with Ce<sup>3+</sup> in C) NN and D) NNN position, E) Au<sup>0</sup>@O, F) Au<sup>0</sup> adsorbed in Ce-Ce bridge position, Au<sup>+</sup> in O-O bridge with Ce<sup>3+</sup> in G) NN, and H) NNN position. CO adsorbed on Au<sub>1</sub>/CeO<sub>2</sub>(111) structures, i.e., CO-Au@O with Ce<sup>3+</sup> in I) NN and J) NNN position. Au<sup>-</sup> adsorbed on the CeO<sub>2-x</sub>(111) surface with Ce<sup>3+</sup> in K) NN and L) NNN position. M) Stable Au<sub>4</sub>/CeO<sub>2</sub>(111) structure, CO

adsorbed on N) Au<sub>top</sub>, O) Au<sub>bottom,1</sub>, and P) Au<sub>bottom,2</sub> positions in Au<sub>4</sub>/CeO<sub>2</sub>(111). Q) Au<sub>3</sub><sup>2+</sup>/Au<sup>-</sup> adsorbed on CeO<sub>2-x</sub>(111). R) Au-CO, S) CO in the gas phase.

**Insight into the reaction mechanism.** In general, the *operando* infrared spectra of the Au/CeO<sub>2</sub> catalyst for CO oxidation can be divided into the carbonate region (800–1800 cm<sup>-1</sup>), the carbonyl region (2000–2300 cm<sup>-1</sup>) discussed in detail above, and the O–H stretching region (>3000 cm<sup>-1</sup>). In the carbonate region, CO<sub>3</sub> carbonates (mainly bidentate: 988, 1298, and 1575 cm<sup>-1</sup>), COOH hydrogen carbonates (1023, 1218, 1393, 1620, and 3619 cm<sup>-1</sup>), and HCOO formates<sup>37,38,51-53</sup> are identified on the catalyst sample, with a strong increase of hydrogen carbonate under reaction conditions after outgassing at 200°C (Figure 4 and Supporting Information). Bidentate carbonates, largely removed by the outgassing treatment, accumulate on the surface with increasing activity of the catalyst, in agreement with the literature.<sup>53</sup> The assignment of these bands is based on a comparison of theory and experiment from previous studies<sup>52</sup> and on isotope exchange experiments using <sup>13</sup>CO (Figure S2) and the corresponding DFT calculations (see Table S1), as described in detail in the Supporting Information.



**Figure 4:** *Operando* diffuse reflectance infrared spectra (carbonate, CO region) of a 0.5 wt% Au/CeO<sub>2</sub> catalyst in 25% O<sub>2</sub> at 21°C recorded directly after equilibration in 25% O<sub>2</sub> (pretreatment A, red), after ~30 min in reaction conditions (2% CO, 10% O<sub>2</sub>, orange), directly after 1 h at 200°C in 25% O<sub>2</sub> (pretreatment B, black), and after ~30 min in reaction conditions (grey). Please note that spectra are offset for clarity.

Moreover, the infrared spectra of the as-prepared (broad band between 3000 and 3500 cm<sup>-1</sup> as well as a band at 3694 cm<sup>-1</sup>) and outgassed catalysts show the presence of adsorbed water; the amount of water is significantly decreased in the case of the outgassed sample (Figures S2 and S3). This behavior indicates that catalyst pretreatment leading to water removal influences the catalyst behavior, as well be discussed below.

To determine potential active gold sites, the temporal behavior of the spectroscopically observed species with respect to the catalyst conversion was studied based on conversion–intensity plots (Figure 5). Figure 5A shows a positive correlation of the band intensity at 2125–2130  $\text{cm}^{-1}$  with the conversion values for both treatments at the initial stage of the reaction, providing direct experimental evidence for CO adsorption at the active site; as the concentration of the active CO species increases, so does the conversion. Actually, as stated above, based on our DFT results, the observed CO stretching frequency at 2125–2130  $\text{cm}^{-1}$  is assigned to CO adsorbed at an isolated gold ion in direct contact with the  $\text{CeO}_2(111)$  surface, thus forming  $\text{O}_{\text{lattice}}\text{-Au}^+\text{-CO}$  species. The calculated frequencies for CO at pseudo–single sites, i.e., gold ions slightly abstracted from a gold cluster<sup>17,28</sup> are predicted to be separated by  $<6 \text{ cm}^{-1}$  from the frequency of a true single site and thus are experimentally not distinguishable: both true and pseudo  $\text{Au}_1$  sites are possible active sites. Thus, by combining *operando* infrared spectroscopy with DFT calculations, the gold active sites for CO oxidation over ceria–supported gold catalysts can be directly observed and identified as isolated  $\text{Au}^+$  for the first time. As shown in Figure 5A, at a later stage, the conversion and band intensity at 2125–2130  $\text{cm}^{-1}$  are not correlated anymore. Thus, when approaching the steady state other aspects of the reaction start to gain importance, which will be the focus of future studies.

We note that the rate-determining step in the CO oxidation reaction over non-hydroxylated ceria-supported gold nanoparticles has been predicted to be the formation of  $\text{COO}_{\text{latt}}$  species, i.e., the abstraction of a lattice oxygen by CO<sup>17,27,28</sup> the activation energy for such a Mars-van-Krevelen mechanism is generally expected to be quite large. However, DFT+U calculations predict values such as 0.86 eV for reaction over  $\text{Au}_1$  single atoms<sup>27</sup>, 0.77 eV over an abstracted atom from a  $\text{Au}_{20}$  cluster<sup>17</sup>, and 0.68 eV over a very flexible  $\text{Au}_3$  cluster<sup>28</sup>. These values of the activation energy, which are lower than expected, are in agreement with the fact that the CO oxidation reaction is facilitated over ceria-supported gold nanoparticles, as observed previously by experiment,<sup>18</sup> although our results now reveal that the



cationic gold active site is formed under reaction conditions at (or separated from) the Au-ceria interface. Thus by directly probing  $O_{\text{lattice}}\text{-Au}^+\text{-CO}$  species prior to the rate-determining step, we can resolve apparent differences in the literature regarding the nature of the active gold site.

As shown in Figure 5A, for both pretreatment procedures, initially a direct relationship is observed, but with different proportionality factors (indicated by the black and red dashed lines). For pretreatment A (red, as-prepared) there is initially a fast activation and later a slow deactivation. In contrast, outgassing pretreatment B (black) results in an activation, that is slow, but finally approaches the same level of conversion ( $\sim 3\%$ ) as for pretreatment A. Interestingly, for both pretreatments deviations from the linearity are observed at a similar CO intensity ( $\sim 1.25$ ) indicating changes in the reaction mechanism at higher CO coverages. Please note that the infrared intensities finally approach each other, indicating the same 'final' concentrations for both experiments (see blue circle for the operation window). Thus, our results strongly suggest, that owing to catalyst structural changes in the presence of the reaction mixture, the catalyst properties approach a common (steady-state) behavior, independent of the initial state.

To elucidate further details of the reaction mechanism, the intensity of the band assigned to CO adsorbed on  $\text{CeO}_2(111)$  at  $2160\text{--}2170\text{ cm}^{-1}$ <sup>37-40</sup> (Figure 5B) and also of the hydrogen carbonate species at  $1218\text{ cm}^{-1}$  (Figure 5C)<sup>50,37,38</sup> were correlated with the catalysts' conversion. Interestingly, for both species, an inverse conversion vs. intensity relationship was found. This behavior strongly suggests that these species act as inhibitors for CO oxidation over Au/CeO<sub>2</sub> catalysts and thus, in their presence, a lowered turnover frequency per active species is expected. This interpretation is consistent with the observation, that under the reaction conditions described above bare ceria did not give any noticeable CO oxidation activity.

As a consequence of the reaction of CO with lattice oxygen, an oxygen vacancy is created. As has been previously proposed<sup>16</sup>, the supply of oxygen occurs by adsorption of molecular oxygen on the oxygen vacancy resulting in the formation of a peroxide species. In the further course of the catalytic cycle the outer oxygen of the peroxide species undergoes

reaction with CO, while the second oxygen fills the oxygen vacancy, closing the catalytic cycle,<sup>17</sup> fully consistent with previous *operando* experiments showing the consumption of peroxide.<sup>14</sup> In this context, the inhibiting effect of the adsorption of CO on the bare support may be explained by the adsorption either on the clean CeO<sub>2</sub>(111) surface, where further reaction, e.g. with residual OH, has been associated with a high barrier (1.05 eV, DFT+U),<sup>54</sup> or on oxygen vacancies on the ceria support, thereby blocking sites accessible to adsorption of molecular oxygen. However, compared to the low adsorption energy of CO at surface oxygen vacancies (−0.4 eV, 2157 cm<sup>−1</sup>, DFT+U),<sup>40</sup> the adsorption of oxygen as peroxide species is more favorable (−1.9 to −2.0 eV, DFT+U),<sup>55–57,34</sup> and therefore oxygen can successfully displace CO (Figure 5B). Note also that the calculated CO stretch frequencies for the clean and reduced surfaces<sup>39</sup> are both consistent with the range of observed frequencies (2160–2170 cm<sup>−1</sup>) differing only by ~12 cm<sup>−1</sup>, hence they are not expected to be distinguishable in our experiment. Previously, CO adsorbed on single-crystalline and defective CeO<sub>2</sub>(111) has been detected at 2054 and 2063 cm<sup>−1</sup>, respectively.<sup>40,58</sup>

As shown in Fig. 5C, the situation is different for hydrogen carbonate species, which also show an inhibiting effect, but are bound much more strongly to the surface than CO (−1.6 eV, see Table S1) and can therefore not be displaced by oxygen that easily. Note that the inhibition of the reaction by the adsorption of CO on the ceria support has not been reported in the literature.<sup>47,34,59</sup> Also, for both inhibiting species their respective concentrations approach a common operation window (indicated by the blue circles in Figure 5), independent of the initial pretreatment. This behavior resembles the behavior observed for the active sites (Figure 5A) and highlights the structural changes of the catalyst in the presence of the gas mixture. Figure 6 summarizes the key features of the proposed mechanism for room temperature CO oxidation over Au/CeO<sub>2</sub> catalysts without participation of water and/or surface hydroxyl groups. For clarity, only the reaction pathway mediated by pseudo–single sites is shown. A crucial step in the catalytic cycle is the formation of CO<sub>2</sub> via O<sub>lattice</sub>-Au<sup>+</sup>-CO species. As a result of the reaction,

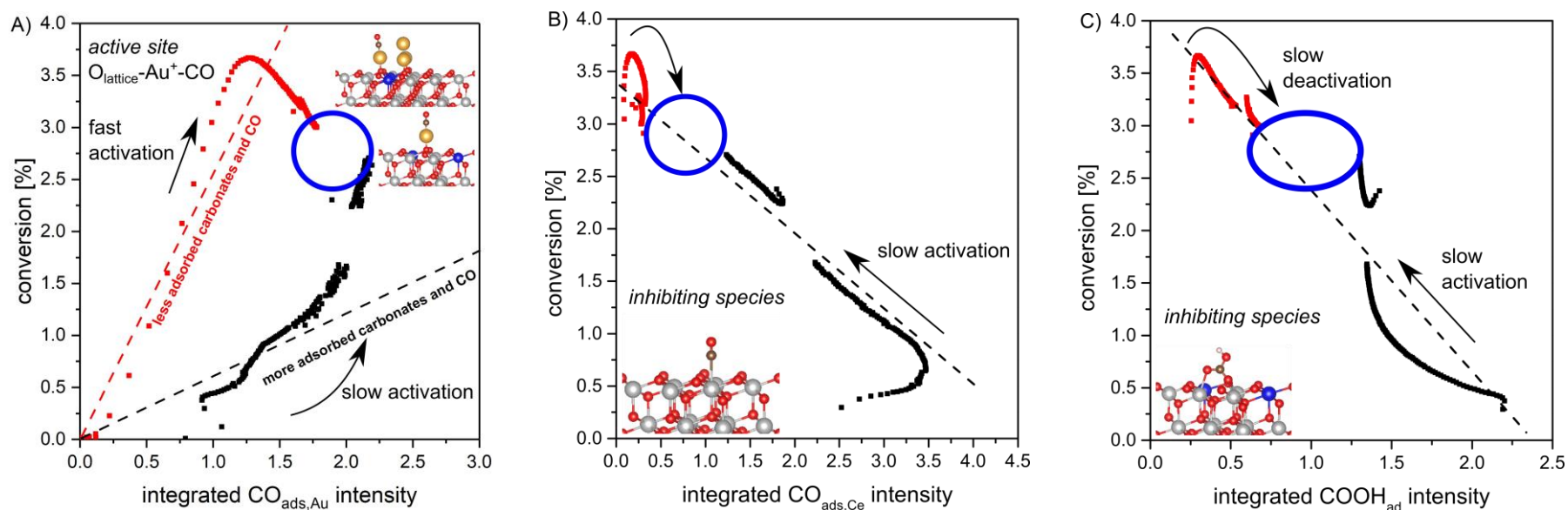
$\text{Au}^-$  is formed as confirmed by Wang et al. for  $\text{Au}_{20}$ .<sup>17</sup> As indicated in Figure 6, the oxygen vacancy created by the oxidation of CO is refilled by gas phase oxygen, while the second oxygen undergoes reaction with CO (see discussion above).

Based on the activity results shown in Figure 1, we conclude that the presence of water facilitates the oxidation of CO, e.g. by catalyzing the reaction between CO and hydroxyl groups via formation of a carboxyl intermediate followed by subsequent  $\text{CO}_2$  and water formation, as proposed both experimentally and theoretically.<sup>38,59,60</sup> Changes in the hydroxyl region (Figure S4) do not show a direct relation to the activity of the catalyst and may result from changes in the coordination of surface water, in agreement with previous studies on CO oxidation over Au/ $\text{TiO}_2$  catalysts.<sup>68</sup> In light of these studies, adsorbed water molecules, rather than support hydroxyl groups, may supply OH for carboxyl formation, followed by its deprotonation to yield  $\text{CO}_2$ .

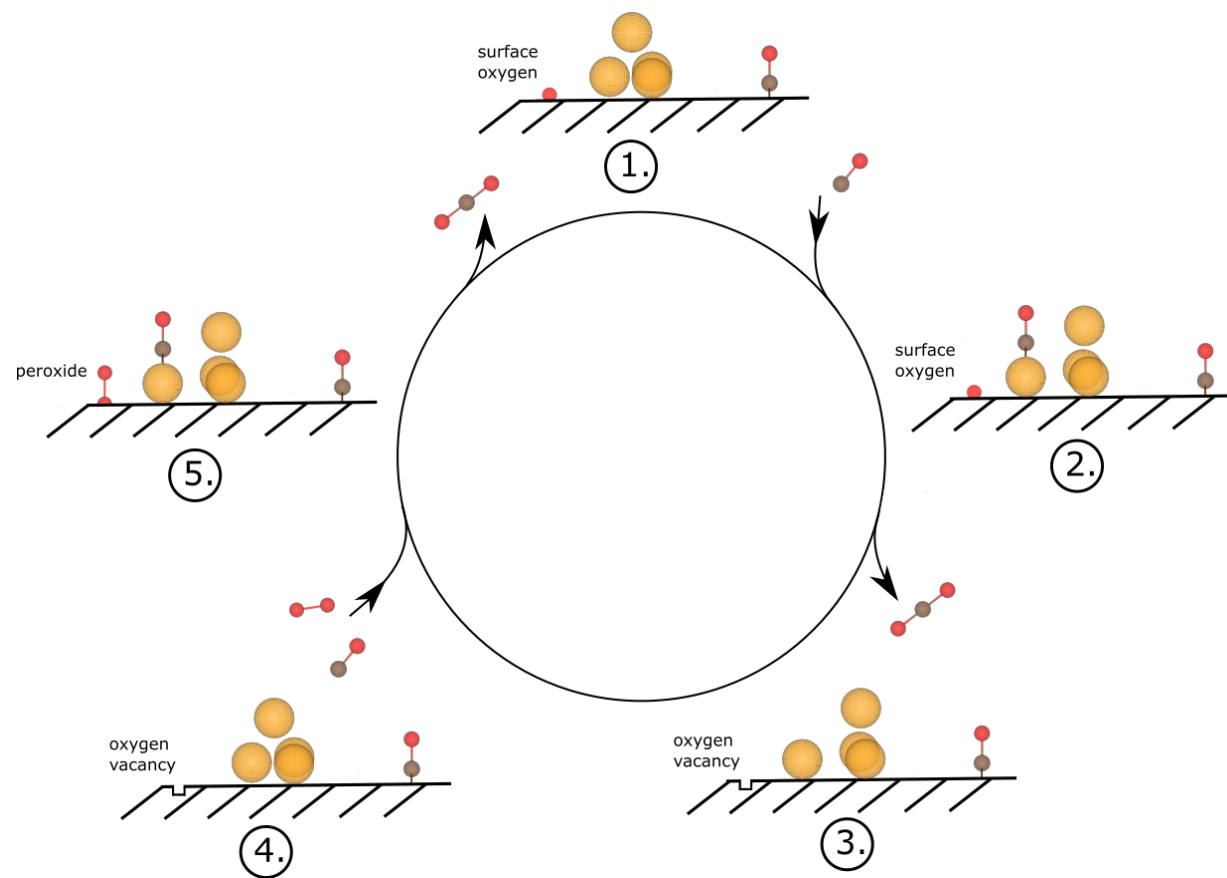
#### 4. Conclusion

In conclusion, cationic gold is evidenced to be an active site of the Au/ $\text{CeO}_2$  catalyst for CO oxidation reactions by using vibrational spectroscopy in conjunction with DFT calculations, which provide a robust foundation for the spectroscopic assignment. The power of this approach is that we could “see” the active  $\text{O}_{\text{lattice}}-\text{Au}^+-\text{CO}$  species. While the experimental frequencies are consistent with the calculated values for CO adsorbed on both single isolated  $\text{Au}^+$  sites and pseudo-single sites, i.e., a gold ion slightly abstracted from a gold cluster, exhibits a lower activation energy in the rate determining step, according to earlier theoretical work.<sup>25</sup> Depending on pretreatment, different reaction / activation regimes were observed providing new insight into the mode of operation of Au/ $\text{CeO}_2$  catalysts during CO oxidation. Higher CO conversion is observed for the as-prepared catalyst, where the inhibiting species, namely, CO adsorbed on the ceria support and hydrogen carbonates, are rare, whereas high concentrations

of these species result in a lower CO conversion, as in the case of the outgassed catalyst. Nevertheless, independent of the pretreatment history, the catalysts approach the same catalytic behavior, but after different times, as is apparent from the conversion–intensity plots, highlighting the structural changes of the catalyst in the presence of the reaction mixture.

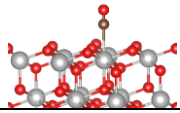

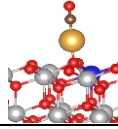
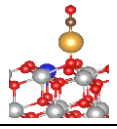
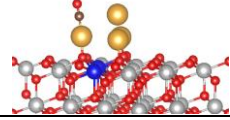
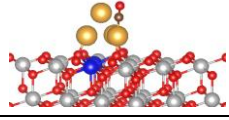
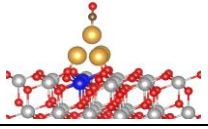


**Figure 5:** A) The intensity of CO adsorbed on Au/CeO<sub>2</sub>(111) (2125 – 2130 cm<sup>-1</sup>) is initially correlated with the conversion of the Au/CeO<sub>2</sub> catalyst for pretreatment A (equilibration in 25% O<sub>2</sub>, red) and pretreatment B (1 h at 200°C in 25% O<sub>2</sub>, black). The dashed lines are a rough interpolation indicating an initial relation between the adsorbed species and the conversion (active site). The black line refers to a high and the red line to a lower concentration of adsorbed CO and carbonate species. The intensity of the band assigned to B) adsorbed CO on the CeO<sub>2</sub>(111) surface (2160–2170 cm<sup>-1</sup>) and to C) hydrogen carbonate adsorbed on CeO<sub>2</sub>(111) (1218 cm<sup>-1</sup>) is correlated to the conversion of the Au/CeO<sub>2</sub> catalyst. The dashed lines in B) and C) show the indirect relation between the adsorbed species and the conversion (inhibiting species). The blue circle is the steady state (operation window) that is approached from two sides for the two pretreatment procedures.



**Figure 6:** Proposed mechanism for the room temperature CO oxidation over Au/CeO<sub>2</sub> catalysts. For clarity, only the reaction pathway mediated by pseudo-single sites is shown. For details see text.

**Table 1:** Summary of the calculated and experimental CO stretch frequency ( $\tilde{\nu}_{\text{CO}}$ ) with respect to the gas phase ( $\Delta\tilde{\nu}_{\text{CO,gas}}$ ) employing the PBE+U/4.5 eV and HSE06 functionals. CO adsorption on CeO<sub>2</sub>(111), Au<sub>1</sub>/CeO<sub>2</sub>(111), and Au<sub>4</sub>/CeO<sub>2</sub>(111) is considered. For Au<sub>1</sub>/CeO<sub>2</sub>(111) two Ce<sup>3+</sup> configurations, and for Au<sub>4</sub>/CeO<sub>2</sub>(111) three non-equivalent CO adsorption sites (top, bottom<sub>1</sub>, and bottom<sub>2</sub>), are considered.

Structure Ce <sup>3+</sup> config. CO ads. site	CO/CeO <sub>2</sub> (111) Ce <sub>top</sub>	CO (gas)	CO- Au <sub>1</sub> /CeO <sub>2</sub> (111) 1×Ce <sup>3+</sup> NN <sup>a</sup> Au <sub>top</sub>	CO- Au <sub>1</sub> /CeO <sub>2</sub> (111) 1×Ce <sup>3+</sup> NNN <sup>a</sup> Au <sub>top</sub>	CO- Au <sub>4</sub> /CeO <sub>2</sub> (111) 2×Ce <sup>3+</sup> NN <sup>a</sup> Au <sub>bottom,1</sub>	CO- Au <sub>4</sub> /CeO <sub>2</sub> (111) 1×Ce <sup>3+</sup> NN <sup>a</sup> Au <sub>bottom,2</sub>	CO- Au <sub>4</sub> /CeO <sub>2</sub> (111) Au <sub>top</sub>
Structure							
<b>PBE+U/4.5 eV</b>							
E <sub>ads,CO</sub> [eV]	-0.19		-2.41	-2.51	-1.37	-1.40	-0.92
$\tilde{\nu}_{\text{CO}}$ [cm <sup>-1</sup> ]	2126	2122	2095	2092	2086	2086	2070
$\Delta\tilde{\nu}_{\text{CO,gas}}$ [cm <sup>-1</sup> ]	+4.3	0	-27.3	-30.4	-35.6	-35.4	-52.4
<b>HSE06</b>							
E <sub>ads,CO</sub> [eV]	-0.15		-2.30	-2.43	-1.26	-1.29	-0.77
$\tilde{\nu}_{\text{CO}}$ [cm <sup>-1</sup> ]	2251	2236	2219	2217	2215	2214	2199
$\Delta\tilde{\nu}_{\text{CO,gas}}$ [cm <sup>-1</sup> ]	+15.0	0	-16.3	-18.5	-21.0	-21.8	-36.3
<b>Experimental</b>							
$\tilde{\nu}_{\text{CO}}$ [cm <sup>-1</sup> ]	2160–2170	2143	2130		–	2125	2090
$\Delta\tilde{\nu}_{\text{CO,gas}}$ [cm <sup>-1</sup> ]	+17 – +27	0	-13		–	-18	-53

<sup>a</sup> number of neighboring Ce<sup>3+</sup> ions to the O<sub>lattice</sub>-Au<sup>+</sup>-CO species

## **Acknowledgements**

DFT calculations for this research were conducted using the Lichtenberg high performance computer of the TU Darmstadt. Computer time at the BSC in Barcelona is also acknowledged. We thank Jochen Rohrer and Karsten Albe for support with the VASP code. C.S. gratefully acknowledges the Merck'sche Gesellschaft für Kunst und Wissenschaft e.V. for providing a scholarship. C.H. acknowledges support by the Deutsche Forschungsgemeinschaft (DFG) and M.V.G.-P. acknowledges support by the MINECO-Spain (CTQ2015-71823-R) and the MICINN-Spain (RTI2018-101604-B-I00).

## **Supplementary material**

Detailed information on experimental and theoretical methods; additional experimental and theoretical data.



## References

1. Haruta, M.; Kobayashi, T.; Sano, H.; Yamada, N. Novel Gold Catalysts for the Oxidation of Carbon Monoxide at a Temperature Far Below 0°C. *Chem. Lett.* **1987**, *16*, 405-408.
2. Hutchings, G. J. Vapor Phase Hydrochlorination of Acetylene: Correlation of Catalytic Activity of Supported Metal Chloride Catalysts. *J. Catal.* **1985**, *96*, 292-295.
3. Hashmi, A. S. K.; Hutchings, G. J. Gold Catalysis. *Angew. Chem. Int. Ed.* **2006**, *45*, 7896-7936.
4. Carrettin, S.; Concepción, P.; Corma, A.; López Nieto, J. M.; Puentes, V. F. Nanocrystalline CeO<sub>2</sub> Increases the Activity of Au for CO Oxidation by Two Orders of Magnitude. *Angew. Chem. Int. Ed.* **2004**, *43*, 2538-2540.
5. Fu, Q.; Saltsburg, H.; Flytzani-Stephanopoulos, M. Active Nonmetallic Au and Pt Species on Ceria-Based Water-Gas Shift Catalysts. *Science* **2003**, *301*, 935-938.
6. Malta, G. *et al.* Identification of Single-Site Gold Catalysis in Acetylene Hydrochlorination. *Science* **2017**, *355*, 1399-1403.
7. Qiao, B. *et al.* Highly Efficient Catalysis of Preferential Oxidation of CO in H<sub>2</sub>-Rich Stream by Gold Single-Atom Catalysts. *ACS Catal.* **5**, 6249-6254 (2015).
8. Manzoli, M., Boccuzzi, F., Chiorino, A., Vindigni, F., Deng, W. & Flytzani-Stephanopoulos, M. Spectroscopic features and reactivity of CO adsorbed on different Au/CeO<sub>2</sub> catalysts. *J. Catal.* **245**, 308-315 (2007).
9. Chiorino, A. *et al.* New Insight on the Nature of Catalytically Active Gold Sites: Quantitative CO Chemisorption Data and Analysis of FTIR Spectra of Adsorbed CO and of Isotopic Mixtures. *J. Catal.* **2009**, *262*, 169-176.
10. Guan, Y.; Ligthart, D. A. J. M.; Pirgon-Galin, O.; Pieterse, J. A. Z.; van Santen, R. A.; Hensen, E. J. M. Gold Stabilized by Nanostructured Ceria Supports: Nature of the Active Sites and Catalytic Performance. *Top. Catal.* **2011**, *54*, 424-438.
11. Vindigni, F.; Manzoli, M.; Chiorino, A.; Boccuzzi, F. Catalytically Active Gold Sites: Nanoparticles, Borderline Sites, Clusters, Cations, Anions? FTIR Spectra Analysis of <sup>12</sup>CO and of <sup>12</sup>CO-<sup>13</sup>CO Isotopic Mixtures. *Gold Bull.* **2009**, *42*, 106-112.
12. Widmann, D.; Leppelt, R.; Behm, R. J. Activation of a Au/CeO<sub>2</sub> Catalyst for the CO Oxidation Reaction by Surface Oxygen Removal/Oxygen Vacancy Formation. *J. Catal.* **2007**, *251*, 437-442.

13. Guzman, J.; Carrettin, S.; Corma, A. Spectroscopic Evidence for the Supply of Reactive Oxygen During CO Oxidation Catalyzed by Gold Supported on Nanocrystalline CeO<sub>2</sub>. *J. Am. Chem. Soc.* **2005**, *127*, 3286-3287.
14. Lohrenscheit, M.; Hess, C. Direct Evidence for the Participation of Oxygen Vacancies in the Oxidation of Carbon Monoxide Over Ceria-Supported Gold Catalysts by Using Operando Raman Spectroscopy. *ChemCatChem* **2016**, *8*, 523-526.
15. Schilling, C.; Hess, C. Real-Time Observation of the Defect Dynamics in Working Au/CeO<sub>2</sub> Catalysts by Combined Operando Raman/UV-Vis Spectroscopy. *J. Phys. Chem. C* **2018**, *122*, 2909-2917.
16. Flytzani-Stephanopoulos, M.; Gates, B. C. Atomically Dispersed Supported Metal Catalysts. *Annu. Rev. Chem. Biomol. Eng.* **2012**, *3*, 545-574.
17. Wang, Y.-G.; Mei, D.; Glezakou, V.-A.; Li, J.; Rousseau, R. Dynamic Formation of Single-Atom Catalytic Active Sites on Ceria-Supported Gold Nanoparticles. *Nat. Commun.* **2015**, *6*, 6511.
18. Guo, L.-W. *et al.* Contributions of Distinct Gold Species to Catalytic Reactivity for Carbon Monoxide Oxidation. *Nat. Commun.* **2016**, *7*, 13481.
19. He, Y. *et al.* Size-Dependent Dynamic Structures of Supported Gold Nanoparticles in CO Oxidation Reaction Condition. *Proc. Natl. Acad. Sci. USA* **2018**, *115*, 7700-7705.
20. Wang, X.-L.; Fu, X.-P.; Wang, W.-W.; Ma, C.; Si, R.; Jia, C.-J. Effect of Structural Evolution of Gold Species Supported on Ceria in Catalyzing CO Oxidation. *J. Phys. Chem. C* **2019**, *123*, 9001-9012.
21. Liu, J.-C.; Wang, Y.-G.; Li, J. Toward Rational Design of Oxide-Supported Single-Atom Catalysts: Atomic Dispersion of Gold on Ceria. *J. Am. Chem. Soc.* **2017**, *139*, 6190-6199.
22. Zhou, X. *et al.* Unraveling Charge State of Supported Au Single-Atoms during CO Oxidation, *J. Am. Chem. Soc.* **2018**, *140*, 554-557.
23. Kettemann, F.; Witte, S.; Birnbaum, A.; Paul, B.; Clavel, G.; Pinna, P.; Rademann, K.; Kraehnert, R.; Polte, J. Unifying Concepts in Room-Temperature CO Oxidation with Gold Catalysts. *ACS Catal.* **2017**, *7*, 8247-8254.
24. Saavedra, J.; Doan, H. A.; Pursell, C. J.; Grabow, L. C.; Chandler, B. D. The Critical Role of Water at the Gold-Titania Interface in Catalytic CO Oxidation. *Science*, **345**, 1599-1602.

25. Zhou, Z.; Kooi, S.; Flytzani-Stephanopoulos, M.; Saltsburg, H. The Role of the Interface in CO Oxidation on Au/CeO<sub>2</sub> Multilayer Nanotowers. *Adv. Funct. Mater.* **2008**, *18*, 2801-2807.
26. Han, Z.-K.; Wang, Y.-G.; Gao Y. Catalytic Role of Vacancy Diffusion in Ceria Supported Atomic Gold Catalyst. *Chem. Commun.* **2017**, *53*, 9125-9128.
27. Camellone, M. F.; Fabris, S. Reaction Mechanisms for the CO Oxidation on Au/CeO<sub>2</sub> Catalysts: Activity of Substitutional Au<sup>3+</sup>/Au<sup>+</sup> Cations and Deactivation of Supported Au<sup>+</sup> Adatoms. *J. Am. Chem. Soc.* **2009**, *131*, 10473-10483.
28. Ghosh, P.; Camellone, M. F.; Fabris, S. Fluxionality of Au Clusters at Ceria Surfaces During CO Oxidation: Relationships Among Reactivity, Size, Cohesion, and Surface Defects from DFT Simulations. *J. Phys. Chem. Lett.* **2013**, *4*, 2256-2263.
29. Kim, H. Y.; Lee, H. M.; Henkelman, G. CO Oxidation Mechanism on CeO<sub>2</sub>-Supported Au Nanoparticles. *J. Am. Chem. Soc.* **2012**, *134*, 1560-1570.
30. Noei, H. *et al.* Probing the Mechanism of Low-Temperature CO Oxidation on Au/ZnO Catalysts by Vibrational Spectroscopy. *J. Phys. Chem. C* **2012**, *116*, 11181–11188.
31. Camellone, M. *et al.* Molecular Understanding of Reactivity and Selectivity for Methanol Oxidation at the Au/TiO<sub>2</sub> Interface. *Angew. Chemie Int. Ed.* **2013**, *52*, 5780–5784.
32. Wang, J. *et al.* Formation, Migration, and Reactivity of Au–CO Complexes on Gold Surfaces. *J. Am. Chem. Soc.* **2016**, *138*, 1518–1526.
33. Uchiyama, T. *et al.* Systematic Morphology Changes of Gold Nanoparticles Supported on CeO<sub>2</sub> during CO Oxidation. *Angew. Chemie Int. Ed.* **2011**, *50*, 10157–10160.
34. Schilling, C.; Hess, C. CO Oxidation on Ceria Supported Gold Catalysts Studied by Combined Operando Raman/UV–Vis and IR Spectroscopy. *Top. Catal.* **2017**, *60*, 131-140.
35. Schilling, C.; Hofmann, A.; Hess, C.; Ganduglia-Pirovano, M. V. Raman Spectra of Polycrystalline CeO<sub>2</sub>: A Density Functional Theory Study. *J. Phys. Chem. C* **2017**, *121*, 20834-20849.
36. Zhang, S.; Li, X.-S.; Chen, B.; Zhu, X.; Shi, C.; Zhu, A.-M. CO Oxidation Activity at Room Temperature Over Au/CeO<sub>2</sub> Catalysts: Disclosure of Induction Period and Humidity Effect. *ACS Catal.* **2014**, *4*, 3481-3489.
37. Binet, C.; Daturi, M.; Lavalley, J.-C. IR Study of Polycrystalline Ceria Properties in Oxidised and Reduced States. *Catal. Today* **1999**, *50*, 207-225.

38. Li, C.; Sakata, Y.; Arai, T.; Domen, K.; Maruya, K.-I.; Onishi, T. Carbon Monoxide and Carbon Dioxide Adsorption on Cerium Oxide Studied by Fourier-Transform Infrared Spectroscopy. Part 1.-Formation of Carbonate Species on Dehydroxylated CeO<sub>2</sub>, at Room Temperature. *J. Chem. Soc., Faraday Trans. 1* **1989**, *85*, 929-943.
39. Farra, R. *et al.* Understanding CeO<sub>2</sub> as a Deacon Catalyst by Probe Molecule Adsorption and In Situ Infrared Characterisations. *Phys. Chem. Chem. Phys.* **2013**, *15*, 3454-3465.
40. Yang, C. *et al.* Chemical Activity of Oxygen Vacancies on Ceria: a Combined Experimental and Theoretical Study on CeO<sub>2</sub>(111). *Phys. Chem. Chem. Phys.* **2014**, *16*, 24165-24168.
41. Lustemberg, P. G. *et al.* Diffusion Barriers Block Defect Occupation on Reduced CeO<sub>2</sub>(111). *Phys. Rev. Lett.* **2016**, *116*, 236101.
42. Penschke, C.; Paier, J. Reduction and Oxidation of Au Adatoms on the CeO<sub>2</sub>(111) Surface - DFT plus U Versus Hybrid Functionals. *Phys. Chem. Chem. Phys.* **2017**, *19*, 12546-12558.
43. Zhang, C.; Michaelides, A.; King, D. A.; Jenkins, S. J. Structure of Gold Atoms on Stoichiometric and Defective Ceria Surfaces, *J. Chem. Phys.* **2008**, *129*, 194708.
44. Zhang, C.; Michaelides, A.; Jenkins, S. J. Theory of Gold on Ceria. *Phys. Chem. Chem. Phys.* **2011**, *13*, 22-33.
45. Hernández, N. C.; Grau-Crespo, R.; de Leeuw, N. H.; Sanz, J. F. Electronic Charge Transfer Between Ceria Surfaces and Gold Adatoms: A GGA + U Investigation. *Phys. Chem. Chem. Phys.* **2009**, *11*, 5246-5252.
46. Teng, B.-T.; Wu, F.-M.; Huang, W.-X.; Wen, X.-D.; Zhao, L.-H.; Luo, M.-F. A DFT Study of the Structures of Au<sub>x</sub> Clusters on a CeO<sub>2</sub>(111) Surface. *ChemPhysChem* **2012**, *13*, 1261-1271.
47. Zhang, C.; Michaelides, A.; King, D. A.; Jenkins, S. J. Positive Charge States and Possible Polymorphism of Gold Nanoclusters on Reduced Ceria. *J. Am. Chem. Soc.* **2010**, *132*, 2175-2182.
48. Carrasco, J.; Barrio, L.; Liu, P.; Rodriguez, J. A.; Ganduglia-Pirovano, M. V. Theoretical Studies of the Adsorption of CO and C on Ni(111) and Ni/CeO<sub>2</sub>(111): Evidence of a Strong Metal-Support Interaction. *J. Phys. Chem. C* **2013**, *117*, 8241-8250.
49. Lustemberg, P. G. *et al.* Room-Temperature Activation of Methane and Dry Re-forming With CO<sub>2</sub> on Ni-CeO<sub>2</sub>(111) Surfaces: Effect of Ce<sup>3+</sup> Sites and Metal-Support Interactions on C-H Bond Cleavage. *ACS Catal.* **2016**, *6*, 8184-8191.

50. Daly, H.; Ni, J.; Thompsett, D.; Meunier, F.C. On the Usefulness of Carbon Isotopic Exchange for the Operando Analysis of Metal-Carbonyl Bands by IR Over Ceria-Containing Catalysts. *J. Catal.* **2008**, *254*, 238-243.
51. Vayssilov, G. N.; Mihaylov, M.; Petkov, P. S.; Hadjiivanov, K. I.; Neyman, K. M. Reassignment of the Vibrational Spectra of Carbonates, Formates, and Related Surface Species on Ceria: A Combined Density Functional and Infrared Spectroscopy Investigation. *J. Phys. Chem. C* **2011**, *115*, 23435-23454.
52. Schilling, C.; Hess, C.; Elucidating the Role of Support Oxygen in the Water–Gas Shift Reaction over Ceria-Supported Gold Catalysts Using *Operando* Spectroscopy. *ACS Catal.* **2019**, *9*, 1159–1171.
53. Abd El-Moemen, A.; Abdel-Mageed, A. M.; Bansmann, J.; Parlinska-Wojtan, M.; Behm, R. J.; Kučerová, G. Deactivation of Au/CeO<sub>2</sub> Catalysts During CO Oxidation: Influence of Pretreatment and Reaction Conditions. *J. Catal.* **2016**, *341*, 160-179
54. Wang, Y.-G.; Mei, D.; Li, J.; Rousseau, R. DFT+U Study on the Localized Electronic States and Their Potential Role During H<sub>2</sub>O Dissociation and CO Oxidation Processes on CeO<sub>2</sub>(111) Surface. *J. Phys. Chem. C*, **2013**, *117*, 23082-23089.
55. Yang, C. *et al.* O<sub>2</sub> Activation on Ceria Catalysts - The Importance of Substrate Crystallographic Orientation. *Angew. Chem. Int. Ed.* **2017**, *56*, 16399-16404.
56. Schilling, C.; Ganduglia-Pirovano, M. V.; Hess, C. Experimental and Theoretical Study on the Nature of Adsorbed Oxygen Species on Shaped Ceria Nanoparticles. *J. Phys. Chem. Lett.* **2018**, *9*, 6593-6598.
57. Chen, S.; Luo, L.; Jiang, Z.; Huang, W. Size-Dependent Reaction Pathways of Low-Temperature CO Oxidation on Au/CeO<sub>2</sub> Catalysts. *ACS Catal.* **2015**, *5*, 1653-1662.
58. Wöll, C. Structure and Chemical Properties of Oxide Nanoparticles Determined by Surface-Ligand IR spectroscopy. *ACS Catal.* **2020**, *10*, 168-176.
59. Wang, C.; Gu, X; Yan, H.; Lin, Y.; Li, J.; Liu, D.; Li, W.-X., Lu, J. Water-Mediated Mars–Van Krevelen Mechanism for CO Oxidation on Ceria-Supported Single-Atom Pt<sub>1</sub> Catalyst. *ACS Catal.* **2017**, *7*, 887-891.
60. Lustemberg, P. G.; Feria, L.; Ganduglia-Pirovano, M. V. Single Ni Sites Supported on CeO<sub>2</sub>(111) Reveal Cooperative Effects in the Water-Gas Shift Reaction. *J. Phys. Chem. C* **2019**, *123*, 7749-7757.
61. Saavedra, J.; Doan, H. A.; Pursell, C. J.; Grabow, L. C.; Chandler, B. D. The Critical Role of Water at the Gold-Titania Interface in Catalytic CO Oxidation. *Science* **2014**, *345*, 1599-1602.

